Phosphoryl transfer reaction snapshots in crystals: Insights into the mechanism of protein kinase A catalytic subunit

Oksana Gerlits,[1] Jianhui Tian,[1] Amit Das,[1] Paul Langan,[1] William T. Heller,[1]* and Andrey Kovalevsky[1]*

[1]Biology and Soft Matter Division, Oak Ridge National Laboratory, Oak Ridge, Tennessee, USA.

*Running title: Catalytic mechanism of protein kinase A

To whom correspondence should be addressed: William T. Heller and Andrey Kovalevsky, Biology and Soft Matter Division, Oak Ridge National Laboratory, Oak Ridge, Tennessee, USA, Tel: (505) 310-4184; E-mail: hellerwt@ornl.gov, kovalevskyay@ornl.gov

Keywords: protein kinase, crystal structure, enzyme mechanism, phosphoryl transfer, molecular dynamics.

Background: PKAc catalyzes phosphorylation of protein substrates thereby regulating a myriad of cellular processes.
Results: X-ray structures of PKAc complexes along the phosphoryl transfer reaction have been obtained.
Conclusion: The phosphotransfer follows a multistep mechanism, including conformational changes of the substrate and product groups, a loose transition state, and metal movement.
Significance: Mechanistic knowledge about the phosphorylation by PKAc will contribute to understanding of the kinase function and regulation.

ABSTRACT

To study the catalytic mechanism of phosphorylation catalyzed by cAMP-dependent protein kinase (PKA) a structure of the enzyme-substrate complex representing the Michaelis complex is of specific interest as it can shed light on the structure of the transition state. However, all previous crystal structures of the Michaelis complex mimics of the PKA catalytic subunit (PKAc) were obtained with either peptide inhibitors or ATP analogs. Here we utilized Ca^{2+} ions and sulfur in place of the nucleophilic oxygen in a 20-residue pseudo-substrate peptide (CP20) and ATP to produce a close mimic of the Michaelis complex. In the ternary reactant complex, the thiol group of the peptide's Cys21 is facing Asp166 and the sulfur atom is positioned for an in-line phosphoryl transfer. Replacement of Ca^{2+} cations with Mg^{2+} ions resulted in a complex with trapped products of ATP hydrolysis: phosphate ion and ADP. Present structural results in combination with the previously reported structures of the transition state mimic and phosphorylated product complexes complete the snapshots of the phosphoryl transfer reaction by PKAc, providing us with the most thorough picture of the catalytic mechanism to date.

INTRODUCTION

Protein kinases are signaling enzymes that regulate cellular processes by catalyzing phosphorylation of proteins. Chemically, protein kinases transfer the γ-phosphoryl group of a nucleotide triphosphate (e.g., ATP) to the hydroxyl group of a serine, threonine, tyrosine or histidine residue of the substrate protein. Over 500 protein kinases have been identified in the human genome (~ 1.7 % of genes), pointing to the biological importance of phosphoryl-transfer chemistry (1). Extensive studies of the cAMP dependent protein kinase (PKA) that phosphorylates the side chains of Ser or Thr residues have made it a paradigm for the whole family of kinase enzymes (2, 3).

Being a regulatory enzyme, PKA is highly regulated itself. When inactive, PKA is a tetrameric holoenzyme, R_2C_2, composed of two catalytic (C) monomeric and regulatory homodimeric (R_2) subunits. An increase in cAMP concentration activates PKA; binding of four cAMP molecules to R_2 causes the tetramer to dissociate, releasing two active C subunits (which we refer to here as PKAc) (4). In PKAc, the nucleotide-binding site is in the cleft between N-terminal and C-terminal lobes that are connected by a small linker region, but the nucleotide primarily interacts with the N-lobe. The substrate sits at the edge of the cleft on the surface of the large C-lobe. PKAc requires one or two divalent

metal ions to bind to the active site to be active (5, 6). The physiological metal is magnesium, although others can support phosphotransferase activity (7, 8).

Crystallographic studies have provided a wealth of information on how PKAc functions (4, 9-11). Complexes of PKAc with nucleotide and/or substrate analogues are found in three major conformational states that differ in the relative orientation of the N- and C-lobes. With no ligands bound (*apo* form) PKAc adopts an open conformation; upon nucleotide or substrate binding (binary form), PKAc transitions to an intermediate, partially closed, state; lastly, PKAc assumes a closed conformation when all components for the reaction are in place (ternary form) (12-15).

Although the PKAc phosphoryl transfer step is fast, > 500 s^{-1}, the product turnover rate is at least an order of magnitude slower; k_{cat} is ~ 20 s^{-1} (16). The rate-limiting step at high Mg concentrations (~10 mM) is the release of MgADP (17). Analysis of the crystallographic structures and solution kinetic data suggests that conformational changes, particularly those involved in the release of the nucleotide, might be essential for PKAc function. Recent nuclear magnetic resonance (NMR) studies and molecular dynamics (MD) simulation have established a relationship between the PKAc conformational fluctuations and its turnover rate (18, 19). Specifically, the rate of the opening motion correlates with k_{cat} and the rate-limiting step – MgADP product release.

The chemical step occurs only in the closed form of PKAc and the release of product is concurrent with the enzyme returning to open conformation. However, single molecule electronic measurements of PKAc catalysis indicate that not every open-close conformational cycle results in the phosphorylation reaction and/or product release, which can partially explain the enzyme's relatively low catalytic efficiency (20). These experiments also caution us on correlating bulk kinetic values, such as the k_{cat}, with the time it takes each individual molecule to go through a particular conformational change or a chemical reaction.

Despite these advances fundamental questions remain unanswered. In particular it is still not clear whether the phosphoryl transfer proceeds as a direct nucleophilic attack by the substrate's OH group on the γ-phosphorus of ATP in the S_N2 fashion or through the metaphosphate intermediate as an S_N1 reaction. Stereochemical NMR studies suggest that PKAc facilitates a direct in-line displacement reaction with the pentacoordinated phosphorus in the transition state (21). Yet, the possibility of the short-lived hindered metaphosphate has not been completely ruled out. Uncertainty also surrounds the roles of active site residues and metal ions, and the details of hydrogen transfer pathways during the chemical step. Specifically, different functions have been proposed for the catalytically important Asp166 residue. In PKAc, Asp166 is the nearest ionizable residue to the substrate's OH group and may act as a catalytic base and/or to correctly position the nucleophile. Asp166 is universally conserved in the active site of all protein kinases and can form hydrogen bond interactions with Ser of the substrate (14, 22, 23). Asp-to-Ala substitution produces a mutant variant with activity below 1% of the wild-type (24).

Several crystallographic structures of PKAc complexes that represent different stages of the phosphoryl transfer reaction have been determined previously. Those mimicking the reactant complexes have been obtained either with peptide inhibitor, IP20, or with unhydrolysable ATP analogs, AMPPCP or AMPPNP. These structures, however, are not very good mimics of the Michaelis complex. In particular, IP20 lacks the nucleophilic group, having Ala in place of reactive Ser, and precluding the analysis of the nucleophile's conformation and interactions before the reaction (15, 25, 26). In addition, in complexes containing substrate peptide SP20 and ATP analogs, the side chain of $Ser21_{SP20}$ adopts a conformation, in which it is rotated away from Asp166 preventing H-bond formation with it (8, 27). The transition state mimic, having the MgF_3^- anion in place of γ-PO_3, ADP and SP20 has also been determined (23). The structure is consistent with the S_N2 mechanism and demonstrates short interaction between Asp166 and the side chain of $Ser21_{SP20}$. Finally, PKAc product complexes have been trapped in crystals when ATP and SP20 were utilized (8). These structures, and enzyme kinetics measurements, demonstrated that, in addition to Mg^{2+}, all other divalent alkaline earth metals, including Ca^{2+}, Sr^{2+} and Ba^{2+}, support the phosphoryl transfer to SP20 (14). In our preliminary studies, the rate of phosphotransfer determined by pre-steady state kinetics for RIIβ holoenzyme in presence of Ca^{2+} is only several-fold lower than with Mg^{2+}. A full kinetic study will be published elsewhere.

In order to design a PKAc complex that more accurately represents the Michaelis complex, inspiration was taken from the near-attack conformation (NAC) theory of enzymes. According to the NAC theory, enzymes may bind substrates with geometries that are very close to those of the transition states (28, 29). NAC is defined as a complex in which reactive groups of substrates and functional groups of an enzyme's active site are in close proximity and in orientation for the reaction to advance. Assuming the structure with MgF_3^- anion

truly mimics the transition state then according to the NAC theory the Michaelis complex should have a similar geometry. The key challenge is in designing the complex to allow all participants in the reaction to assume the correct conformation while preventing the reaction from taking place.

Here we report crystallographic structures of three PKAc complexes. For one, which we designate PKAc-Ca_2ATP-CP20, we co-crystallized PKAc with ATP and a pseudo-substrate peptide (CP20). In CP20 Ser21 of SP20 has been substituted with Cys. For the other, which we designate PKAc-Ca_2AMPPNP-SP20, we co-crystallized PKAc with AMPPNP and a 20-residue substrate analog (SP20). Both were obtained with excess Ca^{2+}. Comparison of the two complexes with the transition state mimic structure reveals fundamental differences in the structures of the active sites that conclusively demonstrate that unhydrolysable ATP analogs produce less biologically-relevant structures of the active site of PKAc, which is supported by our MD simulations of the two structures and the product complex. Specifically, in PKAc-Ca_2ATP-CP20, the thiol group of $Cys21_{CP20}$ is rotated toward Asp166, whereas in PKAc-Ca_2AMPPNP-SP20 the hydroxyl group of $Ser21_{SP20}$ points away from Asp166 into the bulk solvent. This observation indicates that the orientation of the substrate's serine side chain seen in previous crystallographic structures is modulated by ATP analogs. For the third structure, designated as PKAc-Mg_2ADP-PO_4-CP20, the enzyme was crystallized in the presence of ATP, CP20 and Mg^{2+} excess. In PKAc-Mg_2ADP-PO_4-CP20, ATP is completely hydrolyzed into ADP and a free phosphate ion, whereas the side chain of $Cys21_{CP20}$ remains unmodified but occupies two positions.

We propose that because PKAc-Ca_2ATP-CP20 contains reactive ATP, Ca^{2+} ions capable of promoting phosphoryl transfer and a nucleophilic group in the substrate peptide, this complex is the closest model of the actual Michaelis complex to date. In addition we argue that PKAc-Mg_2ADP-PO_4-CP20 can represent a state just after the phosphoryl transfer reaction, but before the phosphorylated $Ser21_{SP20}$ rotates out toward the bulk solvent. Thus, our current results taken together with previously published crystallographic work and theoretical calculations provide the most complete picture to date of the phosphorylation reaction catalyzed by PKAc.

EXPERIMENTAL PROCEDURES

General Information – Pseudo-substrate peptides SP20 (TTYADFIASGRTGRRASIHD; residues 5-24 of the heat-stable PKAc inhibitor PKI, where positions 20 and 21 have been mutated to Ala and Ser) and CP20 (TTYADFIASGRTGRRACIHD; SP20 derivative, where Ser21 was substituted with a Cys residue) were custom-synthesized by Biomatik (Wilmington, Delaware, USA). ATP as the magnesium or disodium salts and AMP-PNP as a lithium salt were purchased from Simga-Aldrich (St. Louis, Missouri, USA). Protein purification supplies were purchased from GE Healthcare (Piscataway, New Jersey, USA). Crystallization reagents were purchased from Hampton Research (Aliso Viejo, California, USA).

Protein Expression and Purification – His_6-tagged recombinant mouse PKAc was expressed in *Escherichia coli* using LB or minimal medium at 18-20°C for 16-18 hrs. The recombinant enzyme was purified by affinity chromatography using HisTrap fast-flow chromatography columns supplied by GE Healthcare. The enzyme was then buffer-exchanged with 50 mM MES, 250 mM NaCl, 2 mM DTT pH 6.5 on a desalting column. Isoforms of PKAc were not separated, without any obvious effect on crystallization of the ternary complexes.

Crystallization – For crystallization trials PKAc was concentrated to 8-12 mg/ml. The ternary complexes with different metals, ATP (or AMP-PNP) and pseudo-substrate peptides CP20 or SP20 were made before setting up crystallization trails. First, the concentrated PKAc solution was mixed with a solution of metal chloride salt to reach the final metal concentration of ~ 20mM. Then the nucleoside was added. The peptide substrate was introduced to the mixture last. The molar ratio of PKAc:Nucleotide:Peptide was kept at 1:10:10. Crystals were grown in sitting drop micro-bridges or in 9-well glass plates using well solutions consisting of 100 mM MES pH 6.5, 5 mM DTT, 15-20% PEG 4000 at 4°C. For complexes with different metal ions, the corresponding metal chloride salts were introduced to the well solutions at 50 mM concentrations prior to setting up crystallization drops.

Data Collection, Structure Determination and Refinement – X-ray crystallographic data were collected at 100K using a Rigaku HomeFlux system, equipped with a MicroMax-007 HF generator, Osmic VariMax optics, and an RAXIS-IV++ image-plate detector. Diffraction data were collected, integrated and scaled using HKL3000 software suite (30). The structures were refined using SHELX-97 (31). A summary of the crystallographic data and refinement is given in Table 1. Similar to our previous observations (25) all the structure were of isoform 2, and contained three post translational phosphorylated residues – Ser139, Thr197, and Ser338. The

structure of the ternary complex of PKAc with $2Mg^{2+}$, ATP and peptide inhibitor IP20 (PDB ID 4DH3) (25) was used as a starting model to solve all the structures described here. The structures were built and manipulated with program *Coot* (32), whereas the figures were generated using the *PyMol* molecular graphics software (v.1.5.0.3; Schrödinger LLC).

Molecular dynamics simulations – MD simulations were performed for PKAc-Ca_2ATP-CP20, PKAc-Ca_2AMPPNP-SP20 and PKAc-Mg_2ADP-pSP20. Briefly, the PKAc-Mg2ATP-IP20 crystal structure (PDB ID 1ATP) (33) was used as a template to set up the simulations. In all three systems, T197 and S338 are phosphorylated with fully ionized phosphate groups. Gromacs-4.6.1(34) was utilized to conduct all the simulations with Amber ff99SB(35) force field with ILDN(36) and NMR(37) modifications. Each of the systems was first energy minimized then a total of 500 ns production simulation was performed under isobaric and isothermal conditions (298 K and 1 atm).

RESULTS

Ternary pseudo-Michaelis complexes PKAc-Ca_2ATP-CP20 and PKAc-Ca_2AMPPNP-SP20 – The electron density maps clearly indicate that intact peptide and nucleotide molecules are trapped in the enzyme active site, confirming the formation of pseudo-Michaelis complexes (Figure 1a, 1b). The two structures are similar, with the RMSD on the main-chain atoms being 0.42 Å, but there are several important structural differences.

In PKAc-Ca_2ATP-CP20, M1 and M2 metals have coordination numbers of seven and six, whereas in PKAc-Ca_2AMPPNP-SP20 both metals are surrounded by eight ligands (Figure 1c). In both structures the coordination spheres around each metal site involve protein residues (Asn171, Asp184) and ATP groups, which are identical to those in the coordination spheres of magnesium, observed previously including PKAc-Mg_2ATP-IP20 complex (PDB ID 4DH3) (15,25,38). The remaining coordination sites around each metal, with the exception of Ca2 in PKAc-Ca_2AMPPNP-SP20, are provided by water molecules. A slight displacement of ~0.5 Å of γ-phosphorus in AMPPNP relatively to ATP puts the former's γ-phosphate closer to M2 site, allowing formation of the second coordination contact between M2 and the γ-phosphate in PKAc-Ca_2AMPPNP-SP20. In addition, a sliding shift of the glycine-rich loop of ~ 1 Å in PKAc-Ca_2AMPPNP-SP20 towards αB helix relative to its position in PKAc-Ca_2ATP-CP20 makes the active site of the former more accessible for water molecules, which explains the increased coordination number of 8 for both Ca^{2+} cations.

In PKAc-Ca_2ATP-CP20, the thiol group of $Cys21_{CP20}$ is facing Asp166. In this orientation the S atom is located in close proximity to the Asp166 carboxyl (S…O distance is of 3.2Å). In contrast, in the PKAc-Ca_2AMPPNP-SP20 structure the Cβ-Oγ bond of $Ser21_{SP20}$ is rotated by ~ 110° away from Asp166, pointing toward the bulk solvent (Figure 1c).

The interactions formed by Lys168 are similar in both structures reported here, but they differ relative to the previously reported PKAc complexes with ATP and IP20 (Figure 1d) (25). Specifically Lys 168 loses direct H-bond interactions with γ-phosphate oxygen of ATP or AMPPNP observed in structures with IP20. The smaller side chain of $Ala21_{IP20}$ lacks a substituent in the γ-position, which allows ATP to move closer to the substrate peptide and to knock out W4 in PKAc-Mg_2ATP-IP20 (Figure 1d).

Comparison of PKAc-Ca_2ATP-CP20, transition state mimic PKAc-Mg_2ADP-MgF_3-SP20 and product PKAc-Ca_2ADP-pSP20 – The previously reported crystal structure of the PKAc with MgADP, SP20, and AlF_3 is considered to be a transition state mimic in the phosphoryl transfer reaction.(23). AlF_3, the transition state analog in place of γ-PO_3, has been reassigned as MgF_3^- anion by Jin et al. (39) based on ^{19}F NMR measurements. Thus, we designate this structure as PKAc-Mg_2ADP-MgF_3-SP20 (PDB ID 1L3R). In addition, we recently obtained an X-ray structure of the complex PKAc-Ca_2ADP-pSP20, in which the ADP and phosphorylated SP20 products were captured in the active site (8). Comparison of our current pseudo-Michaelis complex with the transition state mimic and the product allows us to visualize structural changes that may accompany the catalysis and to identify mechanistically important structural information.

The superposition of the active sites of PKAc-Ca_2ATP-CP20 and PKAc-Mg_2ADP-MgF_3-SP20 is shown in Figure 2. The catalytically important residues occupy very similar positions in both structures, which are aligned with RMSD of 0.55. The main difference is the conformation of the nucleotide's phosphate groups and the displacement of the glycine-rich loop. In PKAc-Ca_2ATP-CP20 the β-P is ~1 Å further away from the metal sites relatively to its position in the transition state mimic, resulting in a 4.1 Å distance between one of the β-P oxygen atoms and Ca2, whereas Mg2 is bound to this oxygen in PKAc-Mg_2ADP-MgF_3-SP20. The geometry of the phosphate groups is reflected in the relative positions of the glycine-rich loop in the two structures (Figure 3). In PKAc-Ca_2ATP-CP20, in addition to a ~ 2 Å sliding displacement, the loop's residues 54 and 55 are positioned more than 2 Å

above their location in PKAc-Mg_2ADP-MgF_3-SP20. Most importantly the side chains of $Ser21_{SP20}$ and $Cys21_{CP20}$ have practically identical conformations, both facing Asp166 and making contacts with its carboxylic oxygen at distances of 2.5 Å and 3.2 Å, respectively.

The active sites of PKAc-Ca_2ATP-CP20 and of the PKAc-Ca_2ADP-pSP20 product complex (PDB ID 4IAK) are geometrically similar, suggesting that the active site organization is same before and after the phosphorylation reaction (Figure 2). The major changes are associated only with the transfer of the γ-phosphoryl group. In the pseudo-Michaelis complex γ-PO_3 is coordinated to both metals and hydrogen bonds to Ser53. In the product complex, γ-PO_3 group moves 2.7 Å, relative to its position in ATP to bind to $Ser21_{SP20}$. The transferred PO_3 group retains its interactions with Ca1 and Ser53, but loses coordination to Ca2. Ca1 maintains 7 ligands in its coordination sphere, whereas Ca2 gains an extra water in the product structure. Another striking difference is the orientation of C_β-S_γ and C_β-O_γ bonds of $Cys21_{CP20}$ and $pSer21_{SP20}$ before and after the reaction. In PKAc-Ca_2ATP-CP20 the side chain of $Cys21_{CP20}$ is oriented toward Asp166, whereas in PKAc-Ca_2ADP-pSP20 C_β-O_γ is rotated away from the active site towards the bulk solvent, which prevents the hydrogen bond from forming between the phosphate group on $pSer21_{SP20}$ and Asp166. The γ-PO_3 transfer is also accompanied by a ~ 2 Å gliding shift of the glycine-rich loop away from the αB helix and towards the metals and ADP (Figure 3).

Ternary complex PKAc-Mg_2ADP-PO_4-CP20 – Although this complex was crystallized using excess of ATP the omit map unmistakably shows that only its hydrolysis products, ADP and PO_4 are present at the enzyme's active site (Figure 4a). Refinement suggested 100 % occupancy for ADP but 64 % for the free phosphate. The partial occupancy of PO_4 is not surprising because small inorganic ions can easily diffuse into the bulk solvent. Additionally, the side chain of Cys21 of CP20 clearly displays two conformations as indicated by the omit difference electron density map, which would not be possible with 100% PO_4 retention. Conformation A (64 % occupancy), in which Cβ-Sγ bond rotated towards bulk solvent and away from Asp166, is similar to that observed in all product complexes (8, 14), and in PKAc-Mg_2AMPPNP-SP20 complex. Conformation B (36 % occupancy) with the SH group pointing towards Asp166 is identical to the position of Cβ-Sγ in PKAc-Ca_2ATP-CP20 and clashing into the free phosphate (Figure 4b). The PKAc-Mg_2ADP-PO_4-CP20 structure agrees very well with the recently published room temperature structure of PKAc-Mg_2ADP-PO_4-IP20 which also demonstrated complete hydrolysis of ATP (25). The two structures are superimposed with RMSD of 0.34 Å.

Molecular Dynamics Simulations – Root mean square deviations (RMSD) for the three simulations showed that all complexes are stable and converged well during our simulation time (Figure 5a). Using the PKAc-Mg_2ATP-IP20 crystal structure as reference, the PKAc-Ca_2AMPPNP-SP20 has the largest RMSD of the three simulations performed. Root mean square fluctuations (RMSF) of the PKAc residues in the complexes are generally small with the exception of the following regions: Lys28 ~ Ala70, Pro236 ~ His260, Val275 ~ Lys295, and Asp328 ~ Glu346. We calculated the distances between the S atom of $Cys21_{CP20}$ and closest O atom in the Asp166 carboxyl in PKAc-Ca_2ATP-CP20 as well as the distance between the O atom in $Ser21_{SP20}$ and closest O atom in Asp166 carboxyl in PKAc-Ca_2AMPPNP-SP20. The S…O distance distribution has a primary peak at 3.5 Å and a minor peak at 7.4 Å, while the O…O distance distribution is broad, spanning from 4.0 Å to 9.0 Å (Figure 5b). For the product complex, the distance between O and Asp166 carboxyl is 6.5±0.9 Å. Finally, PKAc-Ca_2AMPPNP-SP20 complex has the largest radius of gyration, whereas PKAc-Ca_2ADP-pSP20 is the most compact structure (Figure 5c). A characterization of the global motions using principle component analysis indicated that PKAc-Ca_2ATP-CP20 and PKAc-Ca_2ADP-pSP20 have comparable movements related to the opening and closing of the cleft (the dominant motion) that differ from those found in PKAc-Ca_2AMPPNP-SP20 (Figure S6).

DISCUSSION

In this study we utilized Ca^{2+} ions in place of Mg^{2+} and replaced the nucleophilic oxygen in Ser21 of SP20 with sulfur by substituting Cys for Ser to produce a better mimic of the Michaelis complex for the phosphotransfer reaction catalyzed by PKAc. Although a thiol group is a stronger nucleophile than a hydroxyl, thiol analogs are poor kinase substrates (40). Replacement of Ca^{2+} with Mg^{2+} ions in the presence of CP20 substrate analog afforded a complex with trapped phosphate ion. These structures in combination with the previously reported structures of the transition state mimic (23) and product complexes (8, 38) complete the snapshots of the phosphoryl transfer reaction in PKAc.

According to Mildvan's proposal the upper limits of two mechanistically relevant distances, reaction coordinate and axial distances, can be estimated from crystal structures of

phosphotransferase reactant and transition state mimic complexes (41). Analysis of the present results may help discriminate between the dissociative (D_N+A_N, or S_N1) and concerted (A_ND_N, or S_N2) mechanisms, and predict the transition state nature, i.e. loose or tight, for the S_N2 mechanism. In case of PKAc, the reaction coordinate distance can be measured between the nucleophile and γ-P_{ATP} atoms in a Michaelis mimic. The axial distances can be estimated from the Michaelis and transition state mimic structures by dividing the distances between the nucleophile and leaving β-O_{ADP} atoms in half, assuming fully symmetric reaction. As estimated by Mildvan, the reaction coordinate values of ≤ 4.9 Å and the axial distances of ≤ 3.3 Å would indicate the S_N2 mechanism is in operation, whereas longer separations would point to the S_N1 mechanism. The other important parameter is the O-P···O angle between the phosphoryl's P-O bond and the nucleophile atom in the reactant state. If this angle is close to 180°, the reactants are positioned in the near attack configuration for the S_N2 mechanism.

The concerted mechanism has been suggested for PKAc by stereochemical studies (21). Of the two pseudo-Michaelis complex structures reported here the positioning of reactants in the active site of PKAc-Ca_2ATP-CP20 is more consistent with the S_N2 mechanism (Figures 1a and 1b). Specifically, the angle between the $O_β$-$P_γ$ bond of ATP and the S_{Cys21} atom of CP20 is close to linear ($\angle O_{3β}P_γS_{Cys21}$ = 161°). The $C_β$-$S_γ$ bond of $Cys21_{CP20}$ is rotated toward Asp166, making a 3.2 Å hydrogen bond with the carboxylic side chain. Importantly, similar orientation of the side chain of the substrate serine was observed in the structure of the transition state mimic PKAc-Mg_2ADP-MgF_3-SP20 (Figure 2). By contrast in PKAc-Ca_2AMPPNP-SP20 the respective angle ($\angle N_{3β}P_γO_{Ser21}$) is 136° and the serine residue is flipped away from Asp166, facing the bulk solvent. MD simulations demonstrate that $O_γ(Ser_{21})$···$O_δ1$(Asp166) separation covers a wide range from 4.0 Å to 9.0 Å in PKAc-Ca_2AMPPNP-SP20, whereas $S_γ(Cys_{21})$···$O_δ1$(Asp166) distance has a primary peak located at 3.5 Å in PKAc-Ca_2ATP-CP20 (Figure 5b). Based on the previous mechanistic studies, which indicated a possible catalytic role of Asp166 (42, 43), we propose that in PKAc-Ca_2ATP-CP20 the thiol group of $Cys21_{CP20}$ has the correct near-attack conformation that the substrate's serine would assume in the actual Michaelis complex. Notably, only when $C_β$-SH bond assumes the "inward" conformation and interacts with Asp166, sulfur is primed for an in-line phosphoryl transfer, with the $O_β$-$P_γ$···S_{Cys21} angle close to 180°. The reaction coordinate distance $P_γ$···S_{Cys21} measured in PKAc-Ca_2ATP-CP20 is 5.4 Å, which correlates well with that estimated from NMR measurements for the PKAc complex with AMP-PCP and Kemptide (5.3±0.7 Å) (44). The distance between the nucleophilic sulfur and leaving oxygen atoms, $O_β$···S_{Cys21}, is 7 Å, which gives an estimated axial distance of 3.5 Å. These values suggest a very loose transition state and even recommend the formation of the metaphosphate intermediate in the dissociative mechanism S_N1. However, NMR measurements established the inversion of stereochemistry around the γP atom in the product that points to the S_N2 mechanism (21). Yet, S_N1 reactions can also proceed with inversion if an *intimate*, or *tight*, ion pair is formed along the reaction coordinate (45). According to this concept, the metaphosphate intermediate would not diffuse into solvent and would have a short life-time, enough only for vibrational relaxation. Although this idea is appealing, the extended reaction coordinate and axial bond distances can be explained by the larger van der Waals radius of sulfur (1.9 Å) compared to oxygen (1.3 Å) in our study and the use of AMP-PCP in the previous NMR measurements. Indeed, in PKAc-Mg_2ADP-MgF_3-SP20 the axial distances $βO_{ADP}$···MgF_3 and MgF_3···O_{Ser21} are equal, each of 2.3 Å. Assuming the positions of ATP in PKAc-Ca_2ATP-CP20 and Ser21 of SP20 in PKAc-Mg_2ADP-MgF_3-SP20 are representative of the actual Michaelis complex, alignment of the two structures offers considerably shorter distances: 4.4 Å for the reaction coordinate $γP_{ATP}$···O_{Ser21} and 3 Å for the axial distances (Figure 2). These values are similar to those predicted by theoretical calculations for the loose transition state in the S_N2 phosphoryl transfer (46).

The ternary complex PKAc-Mg_2ADP-PO_4-CP20 was prepared in an effort to produce a Michaelis complex mimic containing the physiological Mg^{2+} metal ions. Unexpectedly, products of ATP hydrolysis, ADP and the free phosphate, were found trapped in the active site of PKAc, even though the efficiency of ATP hydrolysis is < 1% of the phosphotransferase activity. Acceleration of ATPase activity was previously observed in the presence of histones, which are natural kinase substrates (47). Moreover, increased ATPase activity has been reported with a pseudo-substrate Leu-Arg-Arg-Ala-Cys-Leu-Gly, whose sequence is similar to that of CP20 and Kemptide (48). Tight binding of IP20 is very efficient in excluding water from the active site resulting in the full inhibition of ATPase activity, which allowed crystallization of ternary PKAc complexes with the unhydrolyzed ATP molecule (15, 25, 26). Nonetheless, two previous crystallographic studies captured the free phosphate in presence of IP20. Full ATP hydrolysis was observed in the room

temperature structure of the wild-type PKAc ternary complex, and was attributed to the X-ray radiation damage (25). Partial ATP hydrolysis was detected in the 100 K structure of the PKAc mutant variant Y204A (49). In this instance, the reaction was attributed to altered conformational dynamics in the mutant.

As a possible explanation for the PKAc ATPase activity it has been suggested that instead of reacting with the nucleophile on the substrate, ATP can be attacked by a water molecule diffused into the enzyme active site and positioned by Asp 166 to initiate the phosphoryl transfer (49). Close inspection of PKAc-Mg_2ADP-PO_4-CP20 and PKAc-Ca_2ATP-CP20 revealed a water molecule that may facilitate ATP hydrolysis by serving as a nucleophile. In the reactant complex, this water labeled as W4 is only 3.9 Å from the γP atom of ATP, forms a hydrogen bond with Asp166 and is also coordinated by Ca2 (Figure 1a and 1c). This water is located at a position nearly identical to an oxygen of the free phosphate in the PKAc-Mg_2ADP-PO_4-CP20 active site (Figure 6). If W4 is, in fact, the nucleophilic water, our structures suggest that prior to the attack this water is activated by the metal ion at M2 and Asp166. In support of this hypothesis, this water molecule is conserved in all of the previously determined product structures, but is absent in ternary PKAc complexes with IP20 (Figure 1d) (25). This observation and the fact that histones increase the PKAc ATPase activity suggests that binding of PKAc natural substrates might not shield its active site from solvent molecules as effectively as does the high-affinity IP20. This is demonstrated in our MD simulation of PKAc-Ca_2ATP-CP20. In the simulation W4 water molecule is dynamic. It occupies the crystallographic position 29% of the simulation time, but can move to nearby positions where it either loses hydrogen bonding to γ-phosphate of ATP or coordination to Ca2, always keeping its hydrogen bonding to Asp166. The water molecule can also leave the active site into the bulk solvent and then return to its original position. It is possible that both the water molecule and the substrate's nucleophilic group are positioned in the reactant complex to attack the γP atom of ATP.

Further analysis of PKAc-Mg_2ADP-PO_4-CP20 leads us to propose that this complex mimics a product state immediately after the phosphoryl transfer takes place, providing insights into the initial step of the product release process. The free phosphate in PKAc-Mg_2ADP-PO_4-CP20 occupies a position similar to that of MgF_3^- in the transition state mimic. In this position the P atom of PO_4 ion is only 1.7 Å and 2.5 Å away from the nucleophilic atoms of the substrate analogs in the transition state mimic and PKAc-Mg_2ADP-PO_4-CP20 structures, respectively. Further, two oxygen atoms of the free phosphate make short interactions with $O_\delta 2$ of Asp166, which implies protonation of either the phosphate ion or Asp166 residue. These interactions are consistent with the Asp166 acting as a base before the phosphoryl is transferred, and also suggests that the proton on Asp166 moves to the phosphoryl group in the product, as predicted by recent QM/MM calculations (50). Protonation of the phosphoryl group would lower the charge on PO_3 from -2 to -1, possibly weakening its interaction with metal ions. This scenario agrees well with the observation that the side chain of pSer21 rotates away from the metals and Asp166 toward the bulk solvent in PKAc-Ca_2ADP-pSP20 after the phosphoryl transfer (8). Comparison of the active sites in PKAc-Ca_2ATP-CP20, PKAc-Mg_2ADP-PO_4-CP20 and PKAc-Ca_2ADP-pSP20 demonstrates that the free phosphate maintains interactions with the metal ions similar to the γ-phosphate of ATP, but the phosphoryl group on pSer21 loses its coordination to M2 (Figure 6). If Asp166 protonates the product's phosphoryl group, it may be an essential first step in the cascade of events necessary for product release, specifically by driving the rotation of the phosphoryl group towards the bulk solvent and opening the glycine-rich loop.

Based on crystallographic evidence Bastidas et al. (38) have suggested that with natural substrates following the phosphorylated product release M1 ion may be expelled from the active site before ADP bound to M2 leaves. Detailed examination of the metal sites' coordination in the previously reported product structures (8) provides additional support for this hypothesis. In the product structures containing Mg^{2+} or Ca^{2+} bound to both M1 and M2 sites the metals are surrounded by the same number of ligands, 6 for Mg^{2+} and 7 for Ca^{2+}. M2 is chelated by the α- and β-phosphates of ADP; M1 has one bond to the β-phosphate of ADP and also is coordinated to the transferred phosphoryl group. Therefore, after the product peptide is released, M1 would have fewer interactions than M2. M1 would interact with Asp184 and the β-phosphate of ADP, whereas M2 would still be chelated by ADP and keep coordination to Asn171 and Asp184.

Analysis of the X-ray structures reported here in combination with the previous structures of the transition state mimic and product complexes permits a detailed description of a possible phosphorylation reaction mechanism. In the Michaelis complex the P-site residue is in the near attack conformation when the side chain faces and makes hydrogen bond with Asp166, as observed in PKAc-Ca_2ATP-CP20 (Figure 7, panel I). The reaction is initiated by the substrate's hydroxyl

nucleophilic attack at the γP_{ATP} and its concurrent deprotonation by Asp166 acting as a base. The reaction proceeds via the concerted S_N2 mechanism with a loose transition state, having the geometry similar to that in PKAc-Mg_2ADP-MgF_3-SP20 (Figure 7, panel II). After the phosphoryl group has been transferred, the phosphorylated product's side chain occupies a position similar to that found for the free phosphate ion in PKAc-Mg_2ADP-PO_4-CP20 (Figure 7, panel III). In this orientation the transferred phosphoryl group would be within hydrogen bonding distance from Asp166. In the next step, Asp166 switches roles to act as an acid that protonates the product's phosphoryl group, which in turn triggers its rotation away from the active site toward solvent (Figure 7, panel IV). The rotation of the phosphoryl group reduces the number of interactions with the active site, including severing coordination to M2 and hydrogen bond with Asp166. As a result a quick product release accompanied by opening of the glycine-rich loop is possible. Following the product release, M1 dissociates. In the final and rate-limiting step, ADP bound to M2 exits the active site, with M2 losing a number of coordination bonds and ADP breaking several hydrogen bonds with the enzyme. The final step would require substantial energy, involving synchronous motions of structural elements in the small lobe (51) and possibly demanding local unfolding of the enzyme (52).

REFERENCES

1. Manning, G., Whyte, D.B., Martinez, R., Hunter, T., Sudarsanam, S. (2002) The Protein Kinase Complement of the Human Genome. *Science* **298**, 1912-1934.

2. Johnson, D. A., Akamine, P., Radzio-Andzelm, E., Madhusudan, and Taylor, S. S. (2001) Dynamics of cAMP-Dependent Protein Kinase. *Chem. Rev.* **101**, 2243-2270.

3. Adams, J. A. (2001) Kinetic and Catalytic Mechanisms of Protein Kinases. *Chem. Rev.* **101**, 2271-2290.

4. Kim, C., Cheng, C. Y., Saldanha, S. A., and Taylor, S. (2007) PKA-I Holoenzyme Structure Reveals a Mechanism for cAMP-Dependent Activation, *Cell* **130**, 1032-1043.

5. Armstrong, R. N., Kondo, H., Granot, J., Kaiser, E. T., and Mildvan, A. S. (1979) Magnetic resonance and kinetic studies of the manganese(II) ion and substrate complexes of the catalytic subunit of adenosine 3',5'-monophosphate dependent protein kinase from bovine heart. *Biochemistry* **18**, 1230-1238.

6. Adams, J. A. and Taylor, S. S. (1993) Divalent metal ions influence catalysis and active-site accessibility in the cAMP-dependent protein kinase. *Protein Sci.* **2**, 2177-2186.

7. Bhatnagar, D., Roskoski, R., Jr., Rosendahl, M. S., and Leonard, N. J. (1983) Adenosine cyclic 3',5'-monophosphate dependent kinase: A new fluorescence displacement titration technique for characterizing the nucleotide binding site on catalytic subunit. *Biochemistry* **22**, 6310-6317.

8. Gerlits, O., Waltman, M. J., Taylor, S., Langan, P., and Kovalevsky, A. (2013) Insights into the Phosphoryl Transfer Catalysed by cAMP-Dependent Protein Kinase: An X-ray Crystallographic Study of Complexes with Various Metals and Peptide Substrate SP20. *Biochemistry* **52**, 3721-3727.

9. Su, Y., Dostmann, W. R., Herberg, F. W., Durick, K., Xuong, N. H., Ten Eyck, L., Taylor, S. S., Varughese, K. I. (1995) Regulatory Subunit of Protein Kinase A: Structure of deletion Mutant with cAMP Binding Domain. *Science* **269**, 807.

10. Kim, C., Xuong, N. H., Taylor, S. S. (2005) Crystal structure of a Complex between the Catalytic and Regulatory (RIα) Subunits of PKA. *Science* **307**, 690

11. Zhang, P., Smith-Nguyen, E. V., Keshwani, M. M., Deal, M. S., Kornev, A. P., Taylor, S. S. (2012) Structure and Allostery of the PKA RIIβ Tetrameric Holoenzyme. *Science* **335**, 712-716.

12. Akamine, P., Madhusudan, Wu, J., Xuong, N.-H., Ten Eyck, L. F. and Taylor, S. S. (2003) Dynamic Features of cAMP-dependent Protein Kinase Revealed by Apoenzyme Crystal Structure. *J. Mol. Biol*. **327**, 159-171.

13. Narayna, N., Cox, S., Xuong, N.-h., ten Eyck, L. F., and Taylor, S. S. (1997) A binary complex of the catalytic subunit of cAMP-dependent protein kinase and adenosine further defines conformational flexibility. *Structure* **5**, 921-935.

14. Gerlits, O., Das, A., Keshwani, M. M., Taylor, S., Waltman, M. J., Langan, P., Heller, W. T., and Kovalevsky, A. (2014) Metal-free cAMP-dependent protein kinase can catalyze phosphoryl transfer. *Biochemistry* **53**, 3179-3186.

15. Zheng, J., Knighton, D., R., Ten Eyck, L. F., Karlsson, R., Xuong, N.-h., Taylor, S. S., and Sowadski, J. M. (1993) Crystal Structure of the catalytic Subunit of cAMP-Dependent Protein Kinase Complexed with MgATP and Peptide Inhibitor. *Biochemistry* **32**, 2154-2161.

16. Grant, B., and Adams, J. A. (1996) Pre-Steady-State Kinetic Analysis of cAMP-Dependent Protein Kinase Using Rapid Quench Flow Techniques. *Biochemistry* **35**, 2022.

17. Shaffer, J. and Adams, J. A. (1999) Detection of Conformational Changes along the Kinetic Pathway of Protein Kinase A Using a catalytic Trapping Technique. *Biochemistry* **38**, 12072-12079.

18. Masterson, L. R., Cheng, C., Yu, T., Tonelli, M., Kornev, A., Taylor, S. S. & Veglia, G. (2010) Dynamics connect substrate recognition to catalysis in protein kinase A. *Nat. Chem. Biol*. **6**, 821-828.

19. Masterson, L. R., Shi, L., Metcalfe, E., Gao, J., Taylor, S. S., and Veglia, G. (2011) Dynamically committed, uncommitted, and quenched states encoded in protein kinase A revealed by NMR spectroscopy. *Proc. Natl. Acad. Sci. USA* **108**, 6969-6974.

20. Sims, P. C., Moody, I. S., Choi, Y., Dong, C., Iftichar, M., Corso, B. L., Gul, O. T., Collins, P. G., and Weiss, G. A. (2013) Electronic measurements of single-molecule catalysis by cAMP-dependent protein kinase A. *J. Am. Chem. Soc.* **135**, 7861-7868.

21. Ho, M.-f., Bramson, N., Hansen, D. E., Knowles, J. R., and Kaiser, E. T. (1988) Stereochemical Course of the Phospho Group Transfer Catalyzed by cAMP-Dependent Kinase. *J. Am. Chem. Soc.* **110**, 2680-2681.

22. Madhusudan, Trafny, E. A., Xuong, N.-H., Adams, J. A., Ten Eyck, L. F., Taylor, S. S., and Sowadski, J. M. (1994) cAMP-dependent protein kinase: Crystallographic insights into substrate recognition and phosphotransfer. *Protein Sci.* **3**, 176-187.

23. Madhusudan, Akamine, P., Xuong, N.-H. and Taylor, S. S. (2002) Crystal structure of a transition state mimic of the catalytic subunit of cAMP-dependent protein kinase. *Nat. Struct. Biol.* **9**, 273-277.

24. Gibbs, C. S. and Zoller, M. J. (1991) Rational Scanning Mutagenesis of a Protein Kinase Identifies Functional Regions Involved in catalysis and Substrate Interactions. *J. Biol. Chem*. **266**, 8923-8931.

25. Kovalevsky, A., Johnson H., Hanson, L., Waltman, M. J., Fisher, Z. S., Taylor, S., Langan, P. (2012) Low and Room Temperature X-ray Structures of Protein Kinase A Ternary Complexes Shed New Light on Its Activity. *Acta Crystallogr., Sect. D: Biol. Crystallogr.* **68**, 854-860.

26. Bossemeyer, D. Engh, R. A., Kinzel, V., Ponstingl, H. and Huber R. (1993) Phosphotransferase and substrate binding mechanism of the cAMP-dependent protein kinase catalytic subunit from porcine heart as deduced from the 2.0 Å structure of the complex with Mn^{2+} adenylyl imidodiphosphate and inhibitor peptide PKI(5-24). *EMBO J.* **12**, 849-859.

27. Bastidas, A. C., Deal, M. S., Steichen J. M., Keshwani, M. M., Guo, Y. and Taylor, S. S. (2012) Role of N-Terminal Myristylation in the Structure and Regulation of cAMP-Dependent Protein Kinase. *J. Mol. Biol.* **422**, 215-229.

28. Bruice, T. C. and Benkovic, S. J. Chemical basis for Enzyme Catalysis. *Biochemistry* **2000**, *39*, 6267-6274.

29. Bruice, T. C. (2002) A View at the Millennium: the Efficiency of Enzymatic Catalysis. *Acc. Chem. Res.* **35**, 139-148.

30. Minor, W., Cymborowski, M., Otwinovski, Z., Chruszcz, M. (2006) HKL3000: the integration of data reduction and structure solution – from diffraction images to an initial model in minutes. *Acta Crystallogr., Sect. D: Biol. Crystallogr.* **62**, 859-866.

31. Sheldrick, G.M. (2008) A short history of SHELX. *Acta Crystallogr., Sect. A: Found. Crystallogr.* **64**, 112-122.

32. Emsley, P., Lohkamp, B., Scott, W.G., Cowtan, K. (2010) Features and development of Coot. *Acta Crystallogr., Sect. D: Biol. Crystallogr.* **66**, 486-501.

33. Zheng, J.; Trafny, E. A.; Knighton, D. R.; Xuong, N. H.; Taylor, S. S.; Ten Eyck, L. F.; Sowadski, J. M. (1993) 2.2 A refined crystal structure of the catalytic subunit of cAMP-dependent protein kinase complexed with MnATP and a peptide inhibitor. *Acta Crystallogr., Sect. D: Biol. Crystallogr.* **49**, 362-365.

34. Pronk, S.; Pall, S.; Schulz, R.; Larsson, P.; Bjelkmar, P.; Apostolov, R.; Shirts, M. R.; Smith, J. C.; Kasson, P. M.; van der Spoel, D.; Hess, B.; Lindahl, E. (2013) GROMACS 4.5: a high-throughput and highly parallel open source molecular simulation toolkit. *Bioinformatics* **29**, 845-854.

35. Hornak, V.; Abel, R.; Okur, A.; Strockbine, B.; Roitberg, A.; Simmerling, C. (2006) Comparison of multiple Amber force fields and development of improved protein backbone parameters. *Proteins* **65**, 712-725.

36. Lindorff-Larsen, K.; Piana, S.; Palmo, K.; Maragakis, P.; Klepeis, J. L.; Dror, R. O.; Shaw, D. E. (2010) Improved side-chain torsion potentials for the Amber ff99SB protein force field. *Proteins: Struct., Funct., Bioinf.* **78**, 1950-1958.

37. Li, D. W.; Bruschweiler, R. (2010) NMR-Based Protein Potentials. *Angew. Chem. Int. Ed. Engl.* **49**, 6778-6780.

38. Bastidas, A. C., Deal, M. S., Steichen, J. M., Guo, Y., Wu, J., and Taylor, S. S. (2013) Phosphoryl Transfer by Protein Kinase A Is Captured in a Crystal lattice. *J. Am. Chem. Soc.* **135**, 4788-4798.

39. Jin, Y., Cliff, M.J., Baxter, N.J., Dannatt, H.R.W., Hounslow, A.M., Bowler, M.W., Blackburn, G.M., Waltho, J.P. (2012) Charge-balanced metal fluoride complexes for protein kinase A with adenosine diphosphate and substrate peptide SP20. *Angew. Chem. Int. Ed*. **51**, 12242-12245

40. Knight, W.B. and Cleland, W.W. (1989) Thiol and Amino Analogues as Alternate Substrates for Glycerokinase from *Candida mycoderma*. *Biochemistry* **28**, 5728-5734.

41. Mildvan, A.S. (1997) Mechanisms of Signaling and Related Enzymes. *Proteins: Struct. Funct. Genet.* **29**, 401-416.

42. Yoon, M.-Y. and Cook, P. F. (1987) Chemical Mechanism of the Adenosine Cyclic 3',5'-Monophosphate Dependent Protein Kinase from pH Studies. *Biochemistry* **26**, 4118-4125.

43. Zhou, J. and Adams, J. A. (1997) Is There a catalytic Base in the Active Site of cAMP-Dependent Protein Kinase? *Biochemistry* **36**, 2977-2984.

44. Granot, J., Mildvan, S. A., Bramson, H. N., and Kaiser, E. T. (1980) Magnetic Resonance Measurements of Intersubstrate Distances at the Active Site of Protein Kinase Using Substitution-Inert Cobalt(III) and Chromium(III) Complexes of Adenosine 5'-(β,γ-Methylenetriphosphate). *Biochemistry* **19**, 3537-3543.

45. Smith, M.B, March, J. (2007) March's Advanced Organic Chemistry: Reactions, Mechanisms, and Structure. John Wiley & Sons, Inc.: Hoboken, NJ, 2357 pp.

46. Valiev, M., Yang, J., Adams, J. A., Taylor, S. S., and Weare, J. H. (2007) Phosphorylation Reaction in cAPK Protein Kinase-Free Energy Quantum Mechanical/Molecular Mechanics Simulations. *J. Phys. Chem. B* **111**, 13455-13464.

47. Moll, G. W., Jr. and Kaiser, E. T. (1976) Phosphorylation of Histone Catalyzed by a Bovine Brain Protein Kinase. *J. Biol. Chem.* **251**, 3993-4000.

48. Mendelow, M., Prorok, M., Salerno, A., and Lawrence, D. S. (1993) ATPase-promoting Dead End Inhibitors of the cAMP-dependent Protein Kinase. *J. Biol. Chem.* **268**, 12289-12296.

49. Yang, J., Eyck, L. F. T., Xuong, N.-H. and Taylor, S. S. (2004) Crystal Structure of a cAMP-dependent Protein Kinase Mutant at 1.26 Å: New Insights into the Catalytic Mechanism. *J. Mol. Biol.* **336**, 473-487.

50. Perez-Gallegos, A., Garcia-Viloca, M., Gonzalez-Lafont, A., and Lluch, J.M. (2015) A QM/MM study of Kemptide phosphorylation catalyzed by protein kinase A. The role of Asp166 as a general acid/base catalyst. Phys. Chem. Chem. Phys. **17**, 3497-3511.

51. Srivastava, A. K., McDonald, L. R., Cembran, A., Kim, J., Masterson, L. R., McClendon, C. L., Taylor, S. S., and Veglia G. (2014) Synchronous opening and closing motions are essential for cAMP-dependent protein kinase A signaling. Structure **22**, 1735-1743.

52. Khavrutskii, I. V.**;** Grant, B., Taylor, S. S., McCammon, J. A. (2009) A Transition Path Ensemble Study Reveals a Linchpin Role for Mg^{2+} during Rate-Limiting ADP Release from Protein Kinase A. *Biochemistry* **48**, 11532-11545.

FOOTNOTES

*AD, JT and WTH were supported and OG and PL were partly supported by a Laboratory Directed Research and Development grant from ORNL. PL was partly supported by an NIH-NIGMS-funded consortium (1R01GM071939-01) between ORNL and LBNL to develop computational tools for neutron protein crystallography. ST was partly supported by NIH grant GM19301.

[1]To whom correspondence should be addressed: Biology and Soft Matter Division, Oak Ridge National Laboratory, Oak Ridge, Tennessee, USA, Tel: (505) 310-4184; E-mail: hellerwt@ornl.gov, kovalevskyay@ornl.gov

[2]Departments of Chemistry/Biochemistry & Pharmacology, University of California San Diego, La Jolla, California, USA.

The structures have been deposited in the PDB and were assigned the following codes: 4XW4 for PKAc-Ca_2AMPPNP-SP20, 4XW5 for PKAc-Ca_2ATP-CP20, and 4XW6 for PKAc-Mg_2ADP-PO_4-CP20.

FIGURE LEGENDS

FIGURE 1. A. Electron density map for the active site components in PKAc-Ca_2ATP-CP20 contoured at 1.5σ level (4σ for calcium cations). B. Electron density map for the active site components in PKAc-Ca_2AMPPNP-SP20 contoured at 1.5σ level (4σ for calcium cations). C. Superposition of the active sites in PKAc-Ca_2ATP-CP20 (colored by atom type, carbon is green, Ca^{2+} ions are dark cyan, H_2O molecules red) and PKAc-Ca_2AMPPNP-SP20 (light magenta carbon atoms, light cyan Ca^{2+} ions, magenta H_2O molecules), showing metals Ca1 and Ca2 bound at sites M1 and M2, respectively, nucleotides ATP and AMPPNP, $Cys21_{CP20}$ and $Ser21_{SP20}$ of the substrate peptides CP20 (blue carbon atoms) and SP20 (orange carbon atoms), respectively, and the residues of the enzyme that are important for metal binding or catalysis. Metal coordination, as black solid lines, and possible hydrogen bonds, as dashed lines, are shown for PKAc-Ca_2ATP-CP20. Distances are in Å. D. Superposition of the active sites in pseudo-Michaelis complexes PKAc-Mg_2ATP-IP20 (PDB: 4DH3, dark magenta for all atoms including Mg^{2+} ions and water molecules), and PKAc-Ca_2ATP-CP20 (carbon colored green, Ca^{2+} ions are dark cyan and water molecules are red). Metal coordination as black solid lines, and possible hydrogen bond as dashed blue are shown for PKAc-Mg_2ATP-IP20. Distances are in Å.

FIGURE 2. Superposition of the active sites in pseudo-Michaelis complex PKAc-Ca_2ATP-CP20 (carbon colored green, Ca^{2+} ions are dark cyan), transition state mimic PKAc-Mg_2ADP-MgF_3-SP20 (PDB ID 1L3R, light pink carbon atoms, magenta Mg^{2+} ions, ball and stick model represents the MgF_3^- anion), and product complex PKAc-Ca_2ADP-pSP20 (blue carbon atoms, light cyan Ca^{2+} ions), showing similar conformation for the side chains of $Ser21_{SP20}$ and $Cys21_{CP20}$, both facing Asp166, whereas in product complex C_β-O_γ is rotated away from Asp166, suggesting the flip of the P-site residue following phosphoryl transfer. The distance between the γ-P of ATP and the oxygen in $Ser21_{SP20}$ is shown as black dashed double arrow. The red dashed arrow demonstrates the difference in the position of γ-PO_3 group before and after the reaction. Distances are in Å.

FIGURE 3. Superposition of the glycine rich loop and the substrate's P-site residue in pseudo-Michaelis complex PKAc-Ca_2ATP-CP20 (carbon colored green), transition state mimic PKAc-Mg_2ADP-MgF_3-SP20 (PDB ID 1L3R, light pink carbon atoms), and product complex PKAc-Ca_2ADP-pSP20 (PDB ID 4IAK, blue carbon atoms) showing different conformations of the glycine rich loop and positions of P-site side chain residue (red and black dashed arrows) relatively to the position of the glycine rich loop at different stages of the phosphoryl transfer reaction.

FIGURE 4. A. $F_O - F_C$ omit difference electron density map for ADP, free phosphate and $Cys21_{CP20}$ in two alternate conformations in PKAc-Mg_2ADP-PO_4-CP20 showing no density for the γ-phosphate of nucleotide. B. A close-up view of the enzyme active site in PKAc-Mg_2ADP-PO_4-CP20 ternary complex showing metals Mg1 and Mg2 bound at sites M1 and M2, respectively, ADP, free phosphate, $Cys21_{CP20}$ of pseudo-substrate peptide in two alternate conformations (blue carbon atoms), and the residues of the enzyme that are important for metal binding or catalysis. Metal coordination is shown as black solid lines, whereas possible hydrogen bonds are represented as blue dashed lines. Distances are in Å.

FIGURE 5. Superposition of the active sites in pseudo-Michaelis complex PKAc-Ca_2ATP-CP20 (carbon colored green, dark cyan Ca^{2+} ions), complex with free phosphate anion PKAc-Mg_2ADP-PO_4-CP20 (yellow carbon atoms, magenta Mg^{2+} ions), and product complex PKAc-Ca_2ADP-pSP20 (PDB ID 4IAK, blue carbon atoms, light cyan Ca^{2+} ions) showing interactions formed by the γ-phosphate and water molecule, W4, at the position of the O3 atom of the free phosphate, in the pseudo-Michaelis (red W4) and the product (blue W4) complexes. Metal coordination is shown as solid lines, whereas possible hydrogen bonds are represented as dashed lines.

FIGURE 6. A. Root mean square deviation (RMSD) of PKA catalytic domain backbone for PKAc-Ca_2ATP-CP20 (red), PKAc-Ca_2AMPPNP-SP20 (blue) and PKAc-Ca_2ADP-pSP20 (PDB ID 4IAK, black) systems is plotted as a function of time. The color scheme is the same for all the following figures. B. Red line shows distribution of distances between S atom of $Cys21_{CP20}$ and closest O atom in Asp166 carboxyl in PKAc-Ca_2ATP-CP20 system. Blue line shows distribution of distances between O atom in $Ser21_{SP20}$ and closest O atom in Asp166 carboxyl in

PKAc-Ca_2AMPPNP-SP20 system. C. Distributions of the radius of gyration calculated for PKAc-Ca_2ATP-CP20, PKAc-Ca_2AMPPNP-SP20 and PKAc-Ca_2ADP-pSP20 systems.

FIGURE 7. Snapshots of the phosphoryl transfer reaction based on crystallographic structures. A close-up view of the enzyme active site in (I) pseudo-Michaelis complex PKAc-Ca_2ATP-CP20 (green, dark cyan Ca^{2+} ions), (II) transition state mimic PKAc-Mg_2ADP-MgF_3-SP20 (PDB ID 1L3R, pink, magenta Mg^{2+} ions), (III) PKAc-Mg_2ADP-PO_4-CP20 ternary complex (yellow, dark magenta Mg^{2+} ions), and (IV) product complex PKAc-Ca_2ADP-pSP20 (PDB ID 4IAK, cyan, cyan Ca^{2+} ions). For (II), (III) and (IV) superposition of the present step (colored by atom type as described above) with the structure of the preceding step shown in blue lines. Water molecules are represented by red and blue spheres for the present and preceding steps, respectively. Metal coordination is shown as solid lines, whereas possible hydrogen bonds are represented as dashed lines.

Table 1. Low temperature X-ray diffraction data collection and refinement statistics.

	LT PKAc-Ca_2ATP-CP20	LT PKAc-Ca_2AMPPNP-SP20	LT PKAc-Mg_2ADP-PO_4-CP20
Data collection			
Space group	$P2_12_12_1$	$P2_12_12_1$	$P2_12_12_1$
Cell dimensions			
a, *b*, *c* (Å)	57.755, 79.331, 98.176	56.364, 78.816, 97.985	57.304, 79.228, 97.820
α, β, γ (°)	90, 90, 90	90, 90, 90	90, 90, 90
Resolution (Å)	40.00 –1.95 (2.02-1.95) *	40.00 – 1.82 (1.89–1.82)	40.00 -1.90 (1.97-1.90)
R_{sym} or R_{merge}	0.047 (0.349)	0.036 (0.467)	0.042 (0.389)
$I / \sigma I$	27.3 (2.4)	33.1 (2.2)	30.2 (2.5)
Completeness (%)	98.0 (91.8)	97.8 (94.4)	98.6 (91.9)
Redundancy	3.9 (3.1)	3.8 (3.1)	3.8 (3.1)
Refinement			
Resolution (Å)	20.00-1.95	20.00-1.82	20.00-1.90
No. reflections	30637	36595	32017
R_{work} / R_{free}	0.185 / 0.252	0.184 / 0.240	0.186 / 0.265
No. atoms			
Protein	2914	2917	2957
Ligand/ion	64	64	65
Water	333	343	377
B-factors	(Ask for input)		
Protein	23.87	23.05	22.81
Ligand/ion	28.79	22.01	28.84
Water	32.56	33.02	32.05
R.m.s. deviations			
Bond lengths (Å)	0.005	0.011	0.015
Angle distances (Å)	0.020	0.027	0.032

*Values in parentheses are for highest-resolution shell.

Figure 1

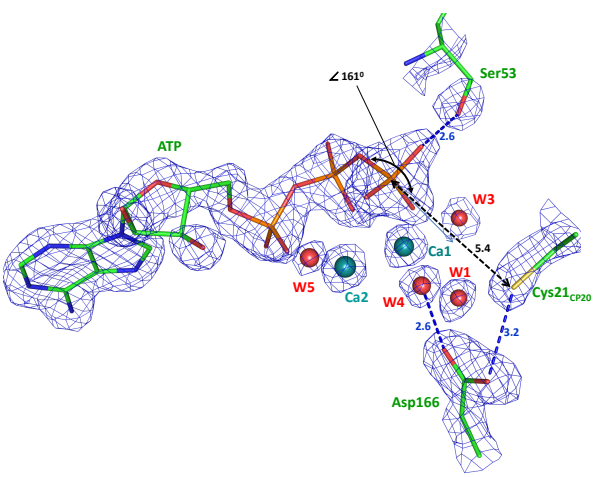

A

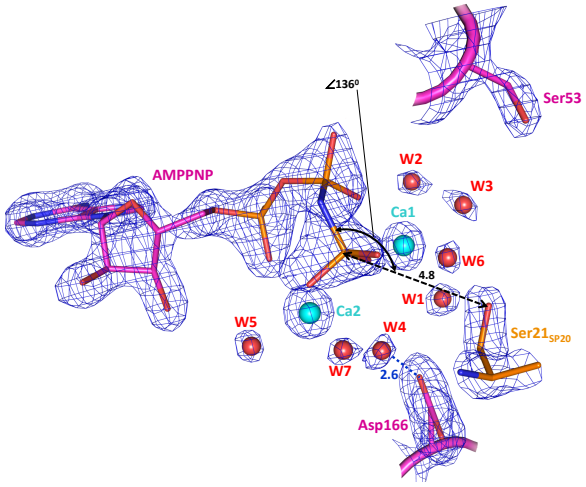

B

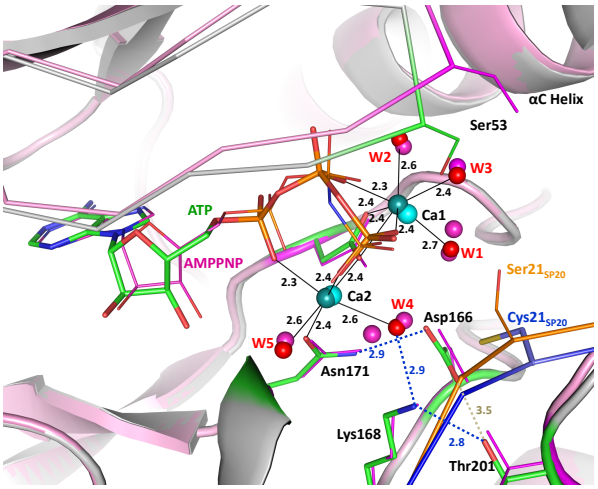

C

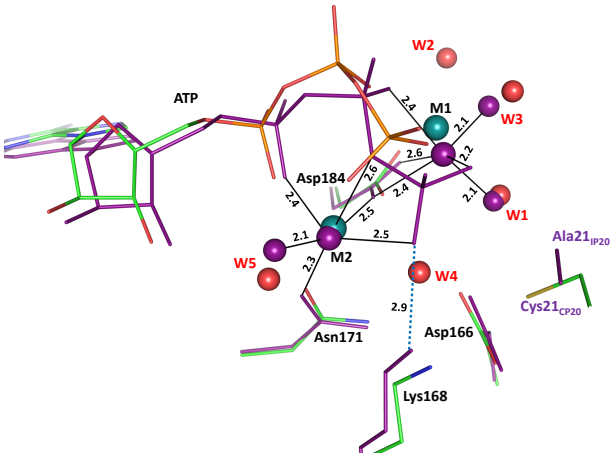

D

Figure 2

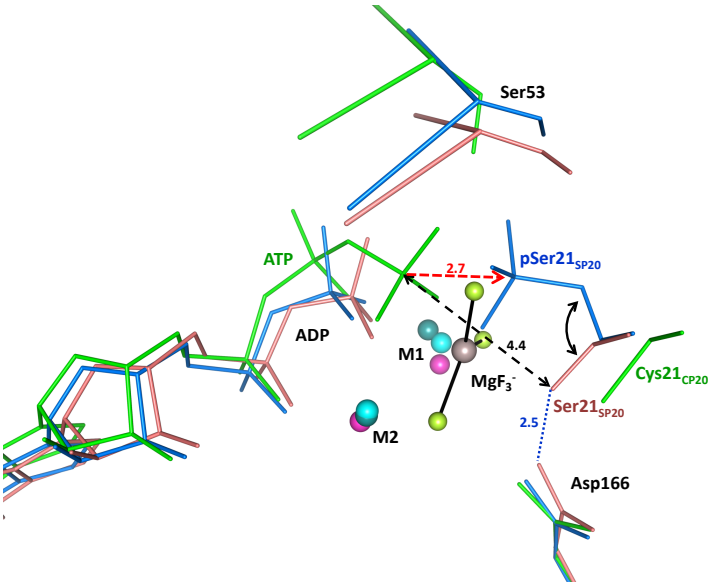
Ser53
ATP
ADP
2.7
pSer21SP20
M1
4.4
MgF3-
Cys21CP20
Ser21SP20
2.5
M2
Asp166

Figure 3

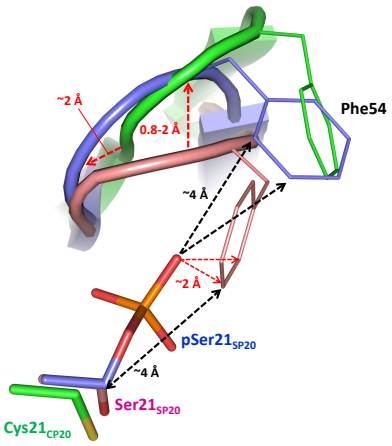

Figure 4

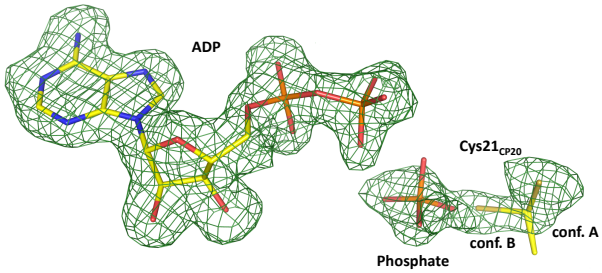
ADP
Cys21CP20
conf. A
conf. B
Phosphate

A

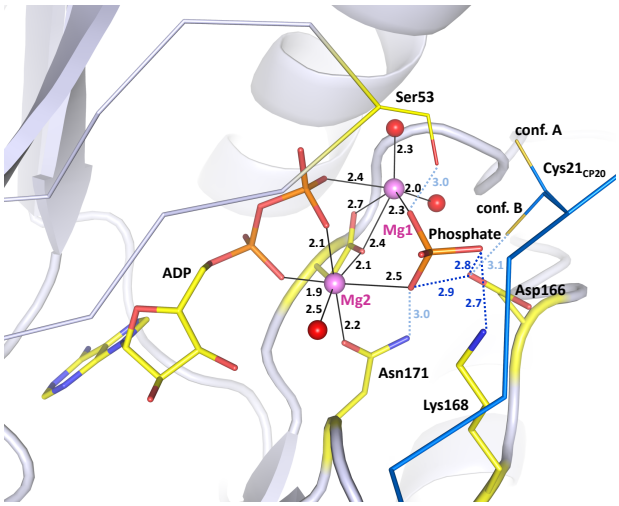
Ser53
conf. A
Cys21CP20
conf. B
Phosphate
Mg1
ADP
Mg2
Asp166
Asn171
Lys168
2.3
2.4
2.0
3.0
2.7
2.3
2.1
2.4
2.1
2.5
2.8
3.1
1.9
2.5
2.9
2.7
2.2
3.0

B

Figure 5

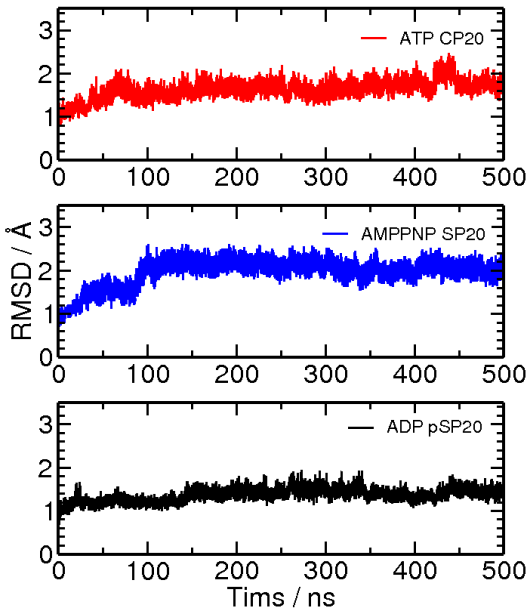
ATP CP20
AMPPNP SP20
ADP pSP20
RMSD / Å
Tims / ns

A

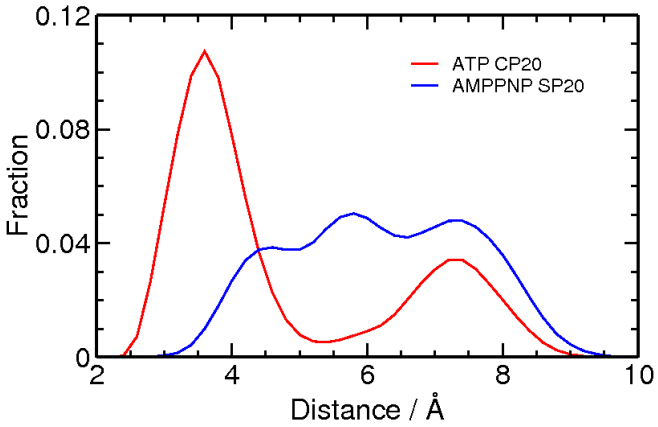
ATP CP20
AMPPNP SP20
Fraction
Distance / Å

B

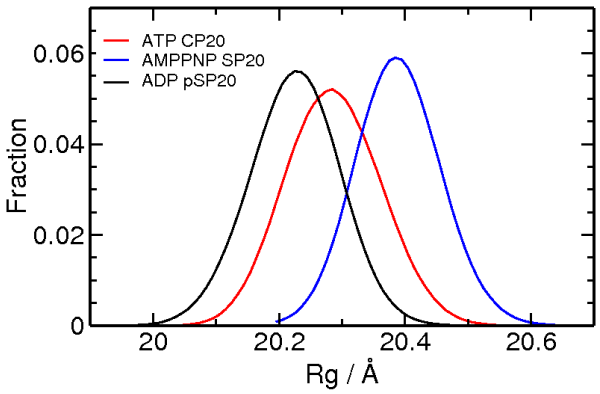
ATP CP20
AMPPNP SP20
ADP pSP20
Fraction
Rg / Å

C

Figure 6

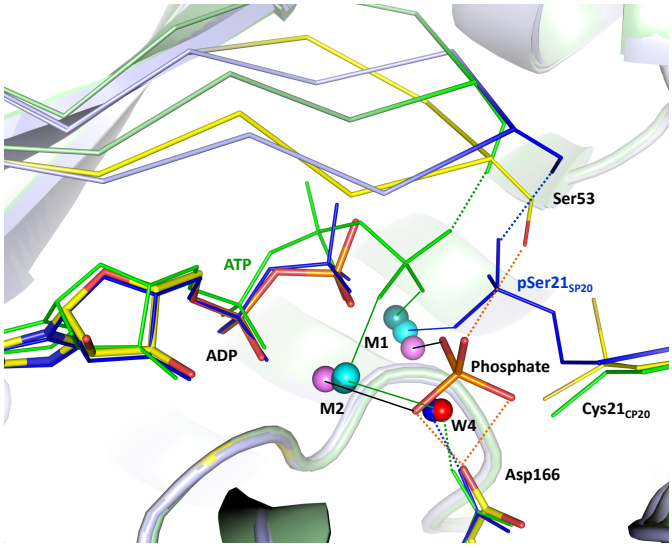
Ser53
ATP
pSer21SP20
ADP
M1
Phosphate
M2
W4
Cys21CP20
Asp166

Figure 7

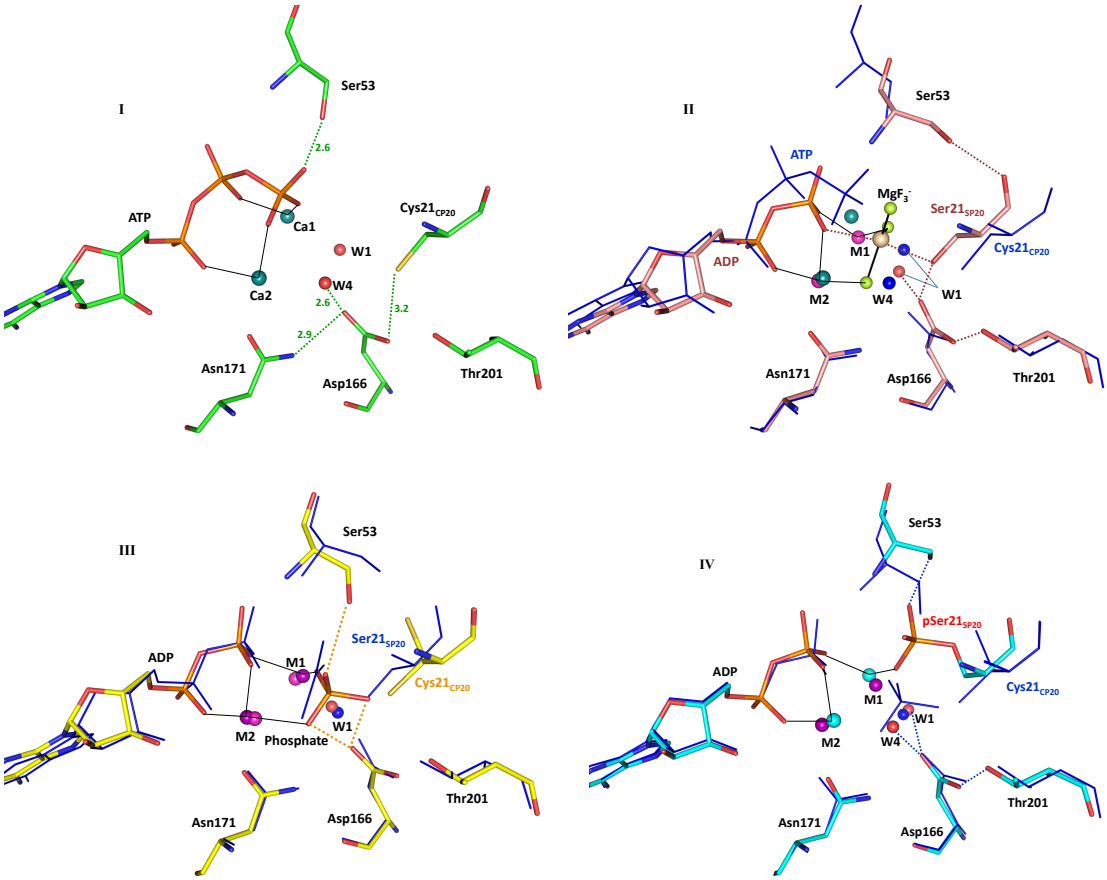
I
Ser53
2.6
ATP
Ca1
Cys21CP20
W1
Ca2
W4
2.6
3.2
2.9
Asn171
Asp166
Thr201
II
Ser53
ATP
MgF3-
Ser21SP20
ADP
M1
Cys21CP20
M2
W4
W1
Asn171
Asp166
Thr201
III
Ser53
Ser21SP20
ADP
M1
Cys21CP20
M2
Phosphate
W1
Asn171
Asp166
Thr201
IV
Ser53
pSer21SP20
ADP
M1
Cys21CP20
W1
M2
W4
Asn171
Asp166
Thr201